

Nanocrystal Arrested Precipitation in Supercritical Carbon Dioxide

Parag S. Shah, Shabbir Husain, Keith P. Johnston,* and Brian A. Korgel*

Department of Chemical Engineering and Texas Materials Institute, Center for Nano- and Molecular Science and Technology, The University of Texas, Austin, Texas 78712-1062

Received: May 11, 2001

Fluorocarbon-coated silver, iridium, and platinum nanocrystals ranging in size from 20 to 120 Å in diameter are synthesized in supercritical (sc)-CO₂ by arrested precipitation from soluble organometallic precursors. The synthesis is performed in a single CO₂ phase by reduction with H₂ at elevated temperatures ranging from 60 to 100 °C. Precursor degradation and particle nucleation occur in the presence of stabilizing perfluorooctanethiol ligands, which bind to the surface of the metal agglomerates and quench particle growth. The ligands are sufficiently solvated by CO₂ to provide a steric barrier to uncontrollable aggregation during synthesis. The particles redisperse in acetone and fluorinated solvents. The dominant mechanism to particle growth is through cluster agglomeration followed by ligand passivation, leading to self-similar size distributions with a standard deviation of ±47%. Additionally, the nanocrystal size is tunable with precursor concentration, with higher precursor loadings resulting in larger nanocrystal sizes.

Introduction

Nanocrystals, 20–100 Å in diameter, exhibit unique size-dependent optical, catalytic, magnetic, and electronic properties compared to their bulk counterparts and could enhance a variety of technologies including coating, environmental, chemical processing, medical, electronic, and sensing applications.^{1–3} Arrested precipitation has proven to be one of the most successful approaches for synthesizing nanocrystals in this size range. This wet chemical synthetic method relies on organic ligands to passivate particle surfaces during growth to provide size control and colloid stabilization. Supercritical fluids (SCF) offer potential advantages over conventional solvents for arrested precipitation synthesis and nanocrystal processing: they exhibit characteristics of both liquids and gases, with sufficient densities (and thus solvent strengths) required for ligand solvation, but with much lower viscosities and higher diffusivities.⁴ SCF density can be altered through modest changes in pressure and temperature. The solvent density strongly influences the interactions between surfactant tails and solvent molecules that are directly responsible for steric stabilization,^{5–7} making SCF solvation characteristics highly *tunable*. Indeed, lattice-fluid theory,^{8,9} Monte Carlo¹⁰ simulation, light scattering¹¹ and neutron scattering¹² have confirmed that colloid steric stabilization in supercritical fluids varies with solvent density. A tunable SCF solvent could provide reversible stabilization and destabilization of colloidal dispersions, which could improve many aspects of nanocrystal processing, such as size-selective separations, synthesis and self-assembly.

Compared to other supercritical fluids, carbon dioxide (CO₂) offers a variety of attractive features. CO₂ is nonflammable, essentially nontoxic, and environmentally benign, and its low critical temperature and pressure of 31 °C and 71 bar, respectively, are easily accessible. There are, however, significant challenges in using sc-CO₂ for arrested precipitation of nanocrystals. CO₂ has a low polarizability per volume (and refractive index) resulting in far weaker van der Waals forces

than those of hydrocarbon solvents, which makes it more like a fluorocarbon.^{13–16} Thus, the key to stabilizing CO₂-based colloidal dispersions of organic¹⁷ and inorganic solids,¹⁸ and water-in-CO₂ microemulsions,¹⁹ has been the design of surfactants with suitable “CO₂-philic” molecular groups to provide the steric barrier to aggregation. Surfactants with fluorinated tails, for example fluoroacrylates, alkanes, and ethers, have proven to be highly effective, as the weak van der Waals forces are consistent with those of CO₂.

Recently, silver²⁰ and cadmium sulfide²¹ nanocrystals were synthesized in water-in-CO₂ microemulsions. In these systems, it can be challenging to recover the particles from the microemulsions without irreversible aggregation because the surfactant is not chemically bound to the nanocrystal surface.²² Shah et al. showed that nanocrystals capped with partially fluorinated thiols (synthesized in an acetone/water mixture using a modification of the biphasic synthesis developed by Brust and co-workers²) disperse in both liquid and supercritical carbon dioxide.²³ Although arrested precipitation has been studied extensively in conventional organic solvents, we have utilized this approach to synthesize sterically stabilized monolayer-protected nanocrystals in CO₂ for the first time.

Here, we report a single-phase sc-CO₂-based arrested precipitation synthesis of silver, platinum, and iridium nanocrystals, 20–120 Å in diameter. Hydrogen is used to reduce an organometallic precursor (silver acetylacetonate (Ag(acac))) for example) in the presence of perfluorooctanethiol, a CO₂-philic capping ligand. The thiolate binds to the nanocrystal surface and carbon dioxide solvates the partially fluorinated hydrocarbon chains. The monolayer of adsorbed ligands surrounding each particle provides steric stabilization of the nanocrystals. The particles can be collected and redispersed in acetone or fluorinated solvents without significant aggregation or increase in particle size. Recently, Watkins and co-workers showed that reduction of organometallic precursors with hydrogen in carbon dioxide leads to highly uniform thin metal films.^{24–26}

Experimental Section

Synthesis. Silver nanocrystals were synthesized in sc-CO₂ by reducing a soluble precursor, silver acetylacetonate

* To whom correspondence should be addressed. Phone: (512) 471-5633. Fax: (512) 471-7060. E-mail: korgel@mail.che.utexas.edu; johnston@che.utexas.edu.

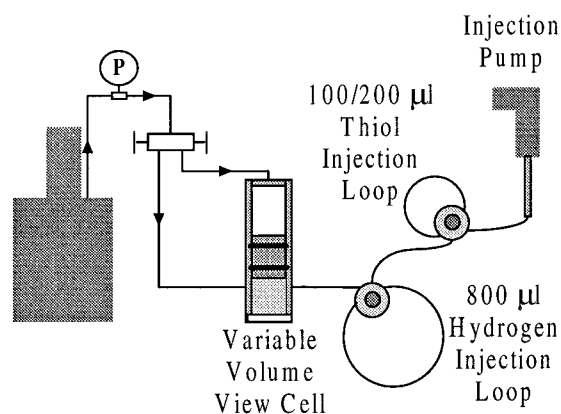


Figure 1. Schematic of reaction apparatus.

(Ag(acac)), Aldrich Chemical Co.), with hydrogen at slightly elevated temperatures ranging from 60 to 100 °C. Iridium and platinum nanocrystals were synthesized using (methylcyclopentadienyl)(1,5-cyclooctadiene)iridium(I) and dimethyl(1,5-cyclopentadiene)platinum(II), respectively (Strem Chemicals, Inc.). A thiolated fluorocarbon molecule, 1*H*,1*H*,2*H*,2*H*-perfluorooctanethiol (Oakwood Products Inc.) (C₆F₁₃C₂H₄SH), was used as the stabilizing ligand. Carbon dioxide (purity > 99.99%) (Matheson Gas Products) and hydrogen (purity > 99.999%) (Praxair, Inc.) were used as received. All reactions were carried out in a temperature-controlled stainless steel, high-pressure variable volume view cell equipped with a piston and a sapphire window in the front and an inside diameter of 1.75 cm.

In a typical experiment, 5.9–16.0 mg of Ag(acac), was loaded into the reaction cell with a working volume (volume with piston in cell) of 27 mL. The cell was sealed and filled with 14–18 mL of CO₂ at 138 bar and 20 °C. The cell was then pressurized to 276 bar with carbon dioxide on the backside of the piston, using a Dionex model 501 Computer Controlled Syringe Pump, and heated to the reaction temperature with heating tape attached to an Omega CN76000 temperature controller. The precursor does not decompose under these conditions. Fluorinated thiol (162–324 mg) and hydrogen (6.22 mg) were simultaneously introduced into the reaction vessel with a high-pressure injection pump through two six-port rotary valves positioned in series (Valco) with attached sample loops. A schematic of the apparatus is shown in Figure 1. The reaction temperature was verified with a thermocouple inserted into the reaction cell, and the pressure was held constant throughout the reaction. The reaction proceeded for 3 h to ensure completion, although visual observation indicated that the inside of the cell reached its darkest after approximately 1 h. After the reaction, the cell was cooled to room temperature and depressurized. CO₂ was then vented as a vapor from the top of the cell, leaving most of the other components other than H₂ in the cell. The nanocrystals were collected from the cell using Omnisolv spectrophotometry grade acetone (EM Science). After collection, the nanocrystals were precipitated using an antisolvent, heptane, to separate unreacted precursor, unbound capping ligands, and undesired reaction byproducts that remained suspended in the supernatant, from the nanocrystals. Nanocrystals were then redispersed in acetone for further analysis. The nanocrystals were also dispersible in fluorinated solvents, such as *Fluorinert brand electronic liquid* and 1,1,2 trichlorotrifluoroethane (Freon).

Characterization. Transmission electron microscopy (TEM) images of the nanocrystals were obtained using a JEOL 2010 high-resolution transmission electron microscope with a 1.7 Å

TABLE 1

exp	precursor concn (mM)	thiol/precursor ratio (mol/mol)	temp (°C)	av nanocrystal diameter (Å)	std dev (Å)	% std dev
A	1.8	14.9	60	39	18	46
B	2.2	10.3	90	26	11	45
C	2.9	8.2	70	50	23	45
D	3.4	6.0	80	57	33	57
E	3.4	5.7	90	55	27	49
F	3.4	6.0	100	59	31	52
G	3.6	5.8	70	56	22	40
H	3.9	6.4	70	69	34	49
I	4.9	11.0	70	107	40	38

point-to-point resolution operating with a 200 kV accelerating voltage and GATAN digital photography system. TEM images were obtained by depositing the nanocrystals on 200 mesh carbon-coated copper grids. Particle size and size distributions were determined using *Scion Image for Windows* software. At least 400 nanocrystals were measured for each sample. Energy-dispersive X-ray spectroscopy (EDS) was performed in situ on a JEOL 2010 TEM equipped with an Oxford Link ISIS EDS instrument.

Results

Silver nanocrystals were synthesized in sc-CO₂ by reducing Ag(acac) at elevated temperatures in the presence of hydrogen and perfluorooctanethiol (see Table 1). The reaction proceeds with hydrogen aiding Ag(acac) reduction to silver, followed by the formation of silver–silver bonds in nucleated clusters of silver atoms. The reaction temperatures listed in Table 1 (60–100 °C) are significantly lower than those typically used (~140 °C) for chemical vapor deposition of metal films using similar precursors.²⁷ The reactivity at low temperatures is a manifestation of the very high solubility of hydrogen and organometallic precursors in CO₂.^{28,29} Perfluorooctanethiol provides steric stabilization and particle size control by binding to the surface of the growing silver particles. Nanocrystals ranged from 26 to 107 Å in average diameter, depending on the precursor concentration (see discussion below). Figure 2a shows a representative TEM image of the silver nanocrystals synthesized in sc-CO₂. Although the particle size distribution was relatively broad with standard deviations about the mean diameter of ±47%, extended regions of hexagonal close packing could still be found in the sample without size fractionation, as seen in Figure 2b. As revealed in the high-resolution TEM image in Figure 2c, the silver nanocrystal cores are crystalline, with the {111} lattice planes visible.

Figure 3 shows the average particle size and polydispersity plotted as a function of initial precursor concentration. Under the conditions explored for the particle growth experiments, the average particle diameter depended strongly on the precursor concentration. As shown in Table 1, the average particle diameter increases from 25 to 107 Å with only a 2-fold increase in Ag(acac) concentration, thus allowing the nanocrystal size to be methodically tuned with changes in the precursor concentration. The polydispersity, however, remained relatively independent of the precursor concentration and average nanocrystal diameter with a standard deviation about the mean diameter of ±47%. Figure 4 shows the average particle size and polydispersity as a function of temperature for experiments D–G. These experiments were done at approximately the same precursor concentration and thiol/precursor ratio. On the basis of these results, it can be seen that neither the final particle size nor the polydispersity is greatly affected by the reaction

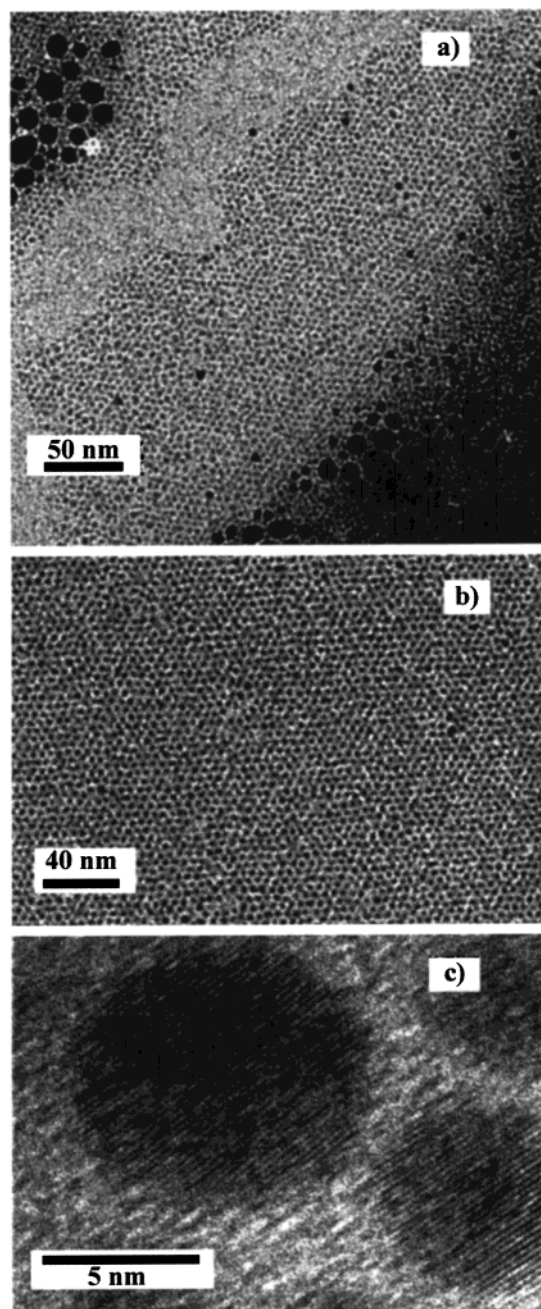


Figure 2. (a) TEM image of silver nanocrystals coated with C₆F₁₃C₂H₄-SH ligands synthesized in CO₂. (b) TEM image of hexagonally close packed array of silver nanocrystals. (c) HRTEM image of silver nanocrystal with visible lattice fringes.

temperature. Figure 5 shows the particle size histograms for reactions A–I.

It is worth noting that the thiol/precursor ratios, which ranged from 6:1 to 15:1, had little effect on the particle size. The thiol/precursor ratios used here are much higher than what is typically used in conventional solvents.^{2,30–32} These experiments were performed in the presence of a large excess of thiol. The large excess of thiol was used to ensure complete surface coverage of the synthesized silver nanocrystals due to the significant challenges in stabilizing particles in sc-CO₂ (see discussion section). A more intensive study would be required to determine the effect of the thiol/precursor ratio on particle size, which is beyond the scope of this work.

The nanocrystals could be repeatedly redispersed in acetone and fluorinated solvents as a result of tight binding of the

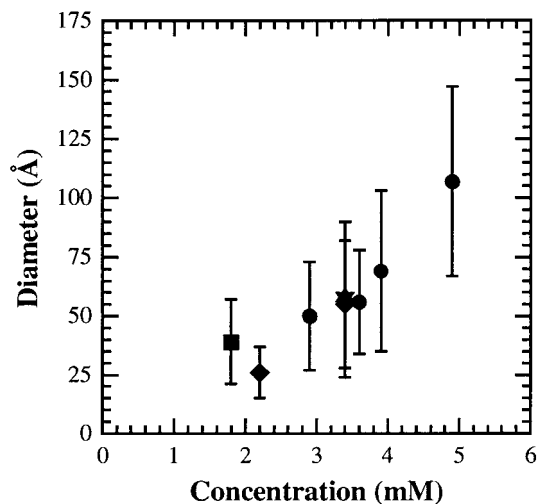


Figure 3. Average nanocrystal diameter vs initial precursor concentration for silver nanocrystals. Error bars correspond to the sample polydispersity, not the uncertainty of the size measurement technique. Nanocrystals synthesized at 60 °C (■), 70 °C (●), 80 °C (▼), 90 °C (◆), and 100 °C (▲).

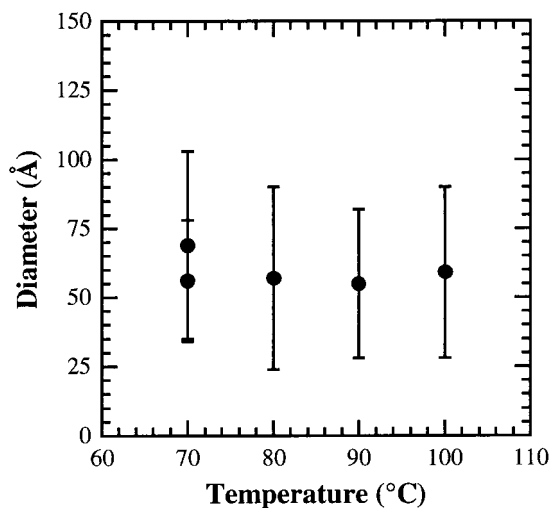


Figure 4. Average nanocrystal diameter vs reaction temperature for experiments D–G. Error bars correspond to the sample polydispersity, not the uncertainty of the size measurement technique.

fluorinated ligands on the nanocrystal surface.²³ The organic molecules maintain a separation between the nanocrystals of approximately 20 Å in the TEM images (Figure 2a for example). The EDS spectra of the silver nanocrystals (Figure 6) confirms the presence of carbon, fluorine, sulfur, and silver in the sample. The interparticle spacing of the perfluorocarbon-coated nanocrystals is significantly larger than the interparticle edge-to-edge separation found for silver nanocrystals coated with octanethiol (~10 Å).³⁰ Self-assembled fluorocarbon monolayers (FSAMs) have been found to be more rigid than hydrocarbon monolayers (SAMs)³³ due to the bulkiness of the fluorine groups. This rigidity decreases the ability of the capping molecules to flex and bend as two nanocrystal cores come together, which leads to larger interparticle separations for fluorocarbon-coated nanocrystals.

The absorbance spectrum of perfluorooctanethiol-capped silver nanocrystals formed in sc-CO₂ shows the characteristic silver surface plasmon resonance (Figure 7) with a maximum absorbance peak at 400 nm.³⁴ This spectrum is similar to the absorbance spectrum of perfluorodecanethiol-capped silver nanocrystals synthesized by reducing silver nitrate in an acetone/

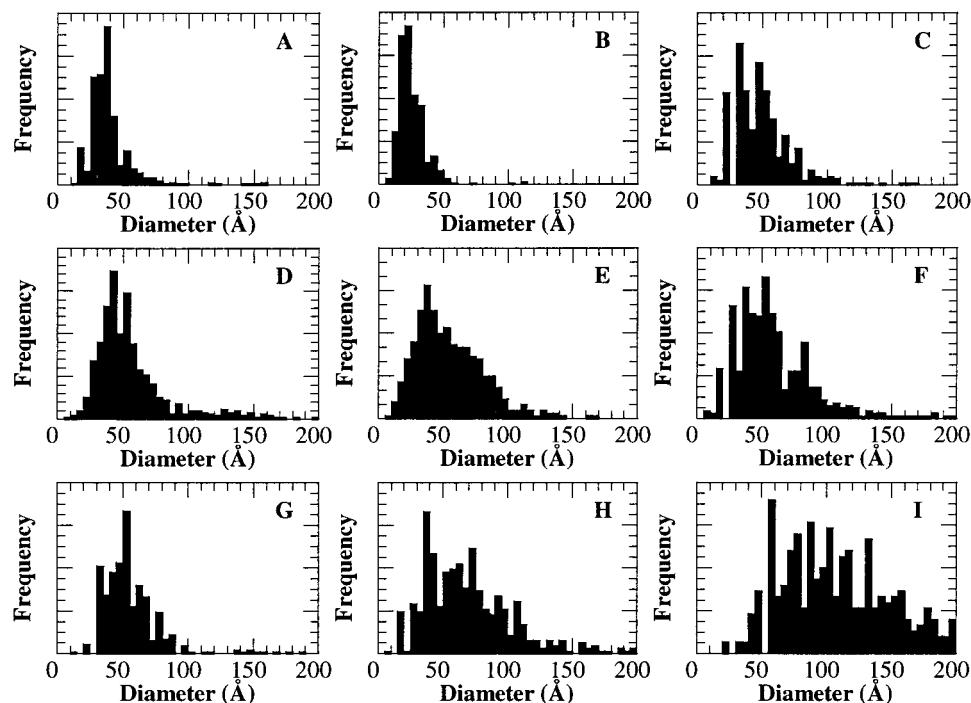


Figure 5. (a)–(i) Silver nanocrystal size distributions for experiments A–I.

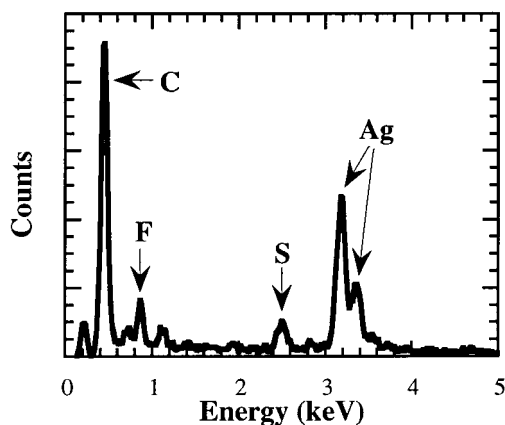


Figure 6. EDS spectra of silver nanocrystals coated with perfluorooctanethiol ligand.

water solution.²³ The difference in peak width between the two spectra results from a difference in particle size between the two samples;³⁴ the nanocrystals formed in acetone are slightly smaller, $d = 55 \text{ \AA}$, compared to the nanocrystals made in CO_2 , $d = 59 \text{ \AA}$. More distinctly, however, the fluorocarbon-coated nanocrystals exhibit a much broader absorbance peak than dodecanethiol-capped silver nanocrystals approximately equal in size. Most likely, the extremely high electronegativity of the fluorine groups surrounding the nanocrystals gives rise to a shorter electron mean free path relative to the hydrocarbon-coated particles.²³

Iridium and platinum nanocrystals were synthesized using (methylcyclopentadienyl)(1,5-cyclooctadiene)iridium(I) and dimethyl(1,5-cyclopentadiene)platinum(II), respectively. The reactions in both cases were carried out at $80 \text{ }^\circ\text{C}$ and 276 bar. For iridium, the precursor concentration was 3.3 mM and the thiol/precursor ratio was 7.6:1. In the case of platinum, the precursor concentration was 3.6 mM and the thiol/precursor ratio was 6.6:1. Parts a and b of Figure 8 show TEM images of the iridium and platinum nanocrystals, respectively. Like the silver nanocrystals, these particles exhibit crystalline cores.

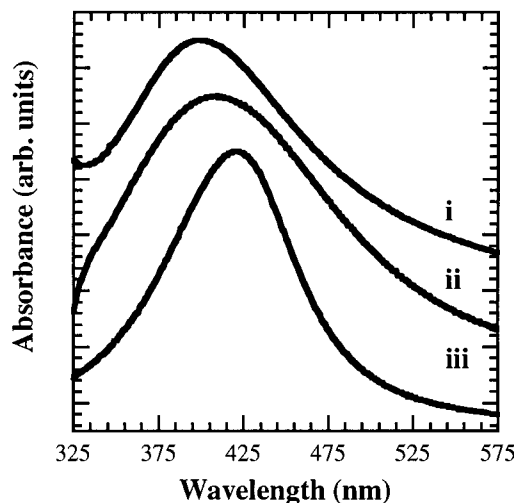


Figure 7. UV–vis absorbance spectra of silver nanocrystals. (i) Nanocrystals formed by $\text{Ag}(\text{acac})$ decomposition in sc-CO_2 with $\text{C}_8\text{F}_{13}\text{C}_2\text{H}_4\text{SH}$, dispersed in acetone. (ii) Nanocrystals formed by AgNO_3 reduction in water/acetone solution with $\text{C}_8\text{F}_{17}\text{C}_2\text{H}_4\text{SH}$, dispersed in acetone. (iii) Nanocrystals formed by AgNO_3 reduction in water/chloroform biphasic solution with $\text{C}_{12}\text{H}_{25}\text{SH}$, dispersed in hexane.

Discussion

Steric Stabilization in CO_2 . Sterically stabilized nanocrystals must exhibit a repulsive force sufficient to overcome the long-range attractive van der Waals force Φ_{vdW} , between particle cores to maintain stability:^{35,36}

$$\Phi_{\text{vdW}} = -\frac{A}{6} \left[\frac{2R^2}{d^2 + 4Rd} + \frac{2R^2}{d^2 + 4Rd + 4R^2} + \ln \left(\frac{d^2 + 4Rd}{d^2 + 4Rd + 4R^2} \right) \right] \quad (1)$$

Equation 1 is valid for two particles of equal radius R , interacting across a medium with an edge-to-edge separation d . The most important parameter in this equation is the Hamaker constant

A , which represents the core–core interaction strength. The Hamaker constant depends on the dielectric constant (ϵ) and refractive index (n) of the particles and the nature of the solvating medium. The Hamaker constant can be estimated using a simplification of Lifshitz theory.³⁷

$$A_{121} = \frac{3}{4}kT \left(\frac{\epsilon_1 - \epsilon_2}{\epsilon_1 + \epsilon_2} \right)^2 + \frac{3h\nu_e}{16\sqrt{2}} \frac{(n_1^2 - n_2^2)^2}{(n_1^2 + n_2^2)^{3/2}} \quad (2)$$

The subscript 1 represents the particles, while 2 represents the solvent medium; h is Planck's constant and ν_e is the maximum electronic ultraviolet adsorption frequency typically assumed to be $3 \times 10^{15} \text{ s}^{-1}$. Using eq 2, CO₂ interactions across a vacuum can be determined by setting ϵ_2 and n_2 to 1. The dielectric constant of silver nanocrystals is size dependent; however, a reasonable estimate can be found by substituting a known value for bulk silver interacting across a vacuum of 2.2 eV.³⁷ Once these two values are determined, the following relationship can be used to determine the Hamaker constant for silver interaction in CO₂.³⁷

$$A_{131} \approx (\sqrt{A_{11}} - \sqrt{A_{33}})^2 \quad (3)$$

A_{131} is for the interaction of two silver cores across CO₂, A_{11} is for silver in a vacuum, and A_{33} is for CO₂ across a vacuum. Silver interactions in CO₂ are very strong due to the large polarizability of the metal and the extremely low polarizability of the solvent. The Hamaker constant for silver in sc-CO₂ at 25 °C is 1.4 eV, compared to 0.93 eV in acetone. Therefore, silver nanocrystals experience nearly 50% stronger attraction in CO₂ than they do in acetone. The increased core–core attraction makes nanocrystal stabilization more difficult in CO₂ than in conventional solvents.

Ligand tails must be well solvated to provide steric stabilization. The chains must protrude into the solvent to enable the molecular fluctuations that give rise to steric repulsion between particles. Fluorination of the hydrocarbon chain induces ligand solvation in CO₂. The repulsive force must overcome Φ_{vdw} to eliminate aggregation; thus, the chain length of the capping ligand is very important for stabilization. In ref 23, C₁₀ perfluorocarbon (C₈F₁₇C₂H₄SH) stabilizing ligands were used, with eight fluorinated carbons and two hydrocarbons adjacent to the thiol. These chains were long enough to enable dispersion of nanocrystals in pure CO₂. In the present study, C₈ perfluorocarbon molecules (C₆F₁₃C₂H₄SH) were used to stabilize the nanocrystals. These chains were sufficient to control particle growth, and flocculation did not occur during the synthesis. However, after collection and washing, the nanocrystals would not redisperse in pure CO₂, despite the fact that they could be redispersed in acetone and fluorocarbon solvents and were well-capped as observed by TEM. It would appear that the perfluorooctanethiol (eight carbons) is simply not long enough to provide redispersibility in CO₂.

The limited stability with C₆F₁₃C₂H₄SH is somewhat unexpected given that octanethiol has been used successfully to sterically stabilize silver nanocrystals in conventional solvents.³⁸ Consider, however, that it is the fluorinated segment of the ligand that CO₂ most effectively solvates, not the CH₂ groups. The fluorinated part of the perfluorooctanethiol ligand is 20% shorter than in the perfluorodecanethiol ligand. In a sense, this is like capping the nanocrystals with a C₆ chain, which simply does not provide sufficient spatial separation (or large enough low cohesive energy density domains) between the particles after

removing the solvent to enable redispersion. Hexanethiol-capped silver nanocrystals, for example, are not easily dispersed in conventional organic solvents; therefore, it is not surprising that perfluorooctanethiol-capped particles with only six fluorocarbons are not easily dispersed in CO₂, which induces even stronger core–core interactions. In polar solvents, however, the steric repulsion provided by the chains appropriately reflects the complete chain length. In acetone and ethanol for example, the large dipole–dipole interactions between the solvent and the CH₂–CF₂ group, which carries a substantial dipole moment, provides the necessary solvation properties for redispersion.³⁹

Growth Mechanism. Hydrogen decomposes the organo-metallic precursor to metal atoms in the presence of perfluorooctanethiol. Chen et al. describe the mechanism for monolayer-protected nanocrystal formation in solution as a three-step process involving nucleation, growth, and passivation.⁴⁰ For example, silver nanocrystal nucleation occurs as the solution reaches supersaturation and continues until the concentration of silver atoms falls below the saturation limit. Nucleation relieves the excess free energy in the supersaturated solution. The nucleation and growth steps must be temporally separated in order to achieve narrow particle size distributions, and in batch systems, rapid nucleation followed by particle growth typically occurs.^{3,40–42} Once nucleated, the particles may grow by a combination of essentially two different mechanisms: (1) reactant diffusion-limited growth (silver atom condensation on existing particles) or (2) core fusion (coagulation). The organic ligands bind to the particle surfaces and halt particle growth at long times to stabilize nanometer-size particles. At long times relative to the nucleation event, the particle size distribution reaches a self-preserving form that depends on the growth mechanism, independent of the initial size distribution of the particle nuclei.⁴³

Figure 3 shows that the average nanocrystal size increases with increasing precursor concentration. To determine if the precursor concentration affects the particle growth mechanism, the size distributions (shown in Figure 5) can be plotted in a reduced form to determine whether they exhibit self-preserving behavior.^{43–45} Friedlander et al. showed that a convenient similarity transformation using a nondimensional distribution function, $\psi_1(\eta) = n(v)\phi/N_\infty^2$ (where $n(v)$ is the concentration of particles with volume v , and ϕ/N_∞ is the average particle volume), can be plotted to compare size distributions between different systems. The total number of particles N_∞ , and total volume of particles ϕ , are calculated using the relationships $N_\infty = \int_0^\infty n(v) dv$ and $\phi = \int_0^\infty vn(v) dv$. Figure 9 shows $\psi_1(\eta)$ plotted as a function of $\eta = vN_\infty/\phi$, the dimensionless particle volume fraction. The particle diameter data determined experimentally from TEM were converted to volumes by assuming spherical particles. For all of the samples studied, $\psi_1(\eta)$ exhibits self-similar behavior, which indicates that the precursor concentration does not affect the particle growth mechanism.

For certain limiting cases of particle growth mechanism, $\psi_1(\eta)$ has been calculated and can be compared directly with experimental results. Essentially, two growth mechanisms, coagulation and condensation, compete to broaden or sharpen the size distribution. Growth by condensation, also known as diffusion-limited growth, narrows the particle size distribution at long times.^{42,46,47} Coagulation, on the other hand, leads to broad particle size distributions. Essentially, we are interested in determining the extent to which coagulation and condensation control particle growth. The high degree of polydispersity seen in these samples (standard deviation of 47%), along with the

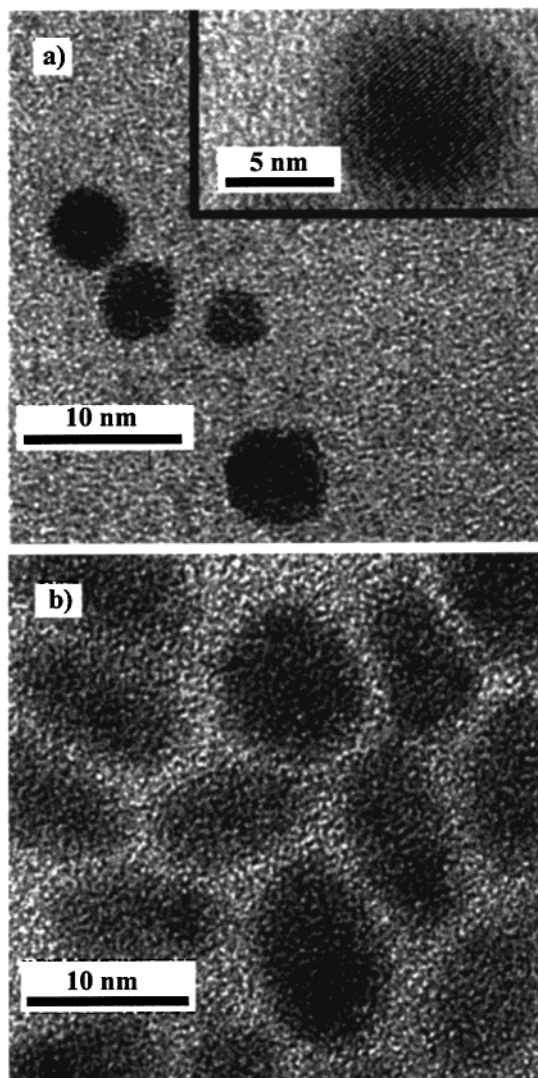


Figure 8. TEM image of (a) iridium nanocrystals coated with $C_6F_{13}C_2H_4SH$ and (b) platinum nanocrystals coated with $C_6F_{13}C_2H_4SH$.

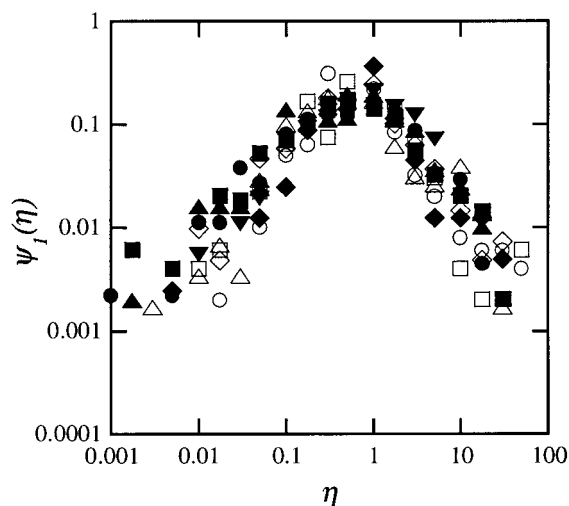


Figure 9. $\psi_1(\eta)$ versus η . Experiments A (○), B (□), C (◇), D (△), E (●), F (■), G (◆), H (▲), and I (▼).

log-normal shape of the size distributions, indicate a coagulation-controlled growth process. Quantitatively, the moments of the size distribution function $\mu_1 = r_3/r_h$ and $\mu_3 = r_1/r_3$ can be used to determine the significance of coagulative growth relative to

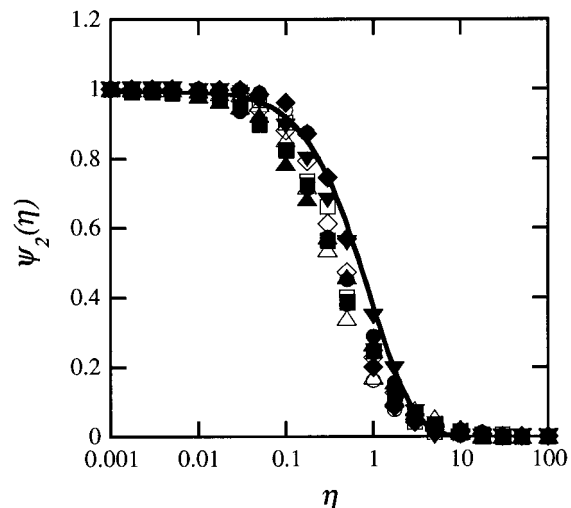


Figure 10. $\psi_2(\eta)$ versus η . Experiments A (○), B (□), C (◇), D (△), E (●), F (■), G (◆), H (▲), and I (▼). $\psi_{2\text{theory}}$ (—) represents the theoretical coagulation solution.

condensation. The parameter r_1 is the arithmetic mean radius defined as $\sum r_i/N_\infty$, r_3 is the cube-mean radius defined as $\sqrt[3]{\sum r_i^3/N_\infty}$, and r_h is the harmonic mean radius defined as $N_\infty/\sum(1/r_i)$. For a monodisperse sample, $r_1 = r_3 = r_h$, and $\mu_1 = \mu_3 = 1$. In our case, the average value for μ_1 is 1.48 and μ_3 is 0.82. Values of $\mu_1 > 1.25$ and $\mu_3 < 0.905$ indicate that coagulation controls growth.

An effective method of comparing size distributions is to compare the nondimensional distribution function, $\psi_2(\eta) = N_v/N_\infty = \int_\eta^\infty \psi_1(\eta) dv$. N_v represents the total number of particles larger than v : $N_v = \int_v^\infty n(v) dv$. In Figure 10, $\psi_2(\eta)$ are plotted as a function of η . Again, the data exhibit a high degree of self-similarity. The theoretically calculated values for $\psi_2(\eta)$ for Brownian coagulative growth at long times, assuming a particle sticking probability of 1, are also plotted in Figure 10. The model calculations agree well with the data apart from a slight variation in the middle of the size distribution. The data skew slightly to a higher average volume. The deviation from the model curve can be interpreted as an indication that the particle sticking probability is less than 1. Given that the particles, particularly at long times, are coated with the organic ligands, a sticking probability less than 1 is expected. Certainly, the sticking probability must decrease essentially to values of zero in order to maintain stable particles.

Figure 11 shows TEM images of polycrystalline silver nanocrystals with multiple misaligned lattice fringes. The internal crystalline domains possibly relate to the initial particle nuclei prior to coagulation. It is important to note, however, that the majority of the particles examined appear to be single crystals, as seen in Figure 2c. Although one might expect all of the particles to be polycrystalline in a system dominated by coagulation, Yacamán and co-workers recently observed atomic reorganization and restructuring in gold particles as large as 70 Å in diameter after coagulation.⁴⁸ In our system, it appears that crystal planes can realign within the nanocrystal core; however, the polycrystallinity resulting from the coagulative growth process persists in some particles.

Conclusions

Fluorocarbon-coated silver, iridium, and platinum nanocrystals ranging in size from 20 to 120 Å in diameter were synthesized in *sc*-CO₂ by arrested precipitation. These fluoro-

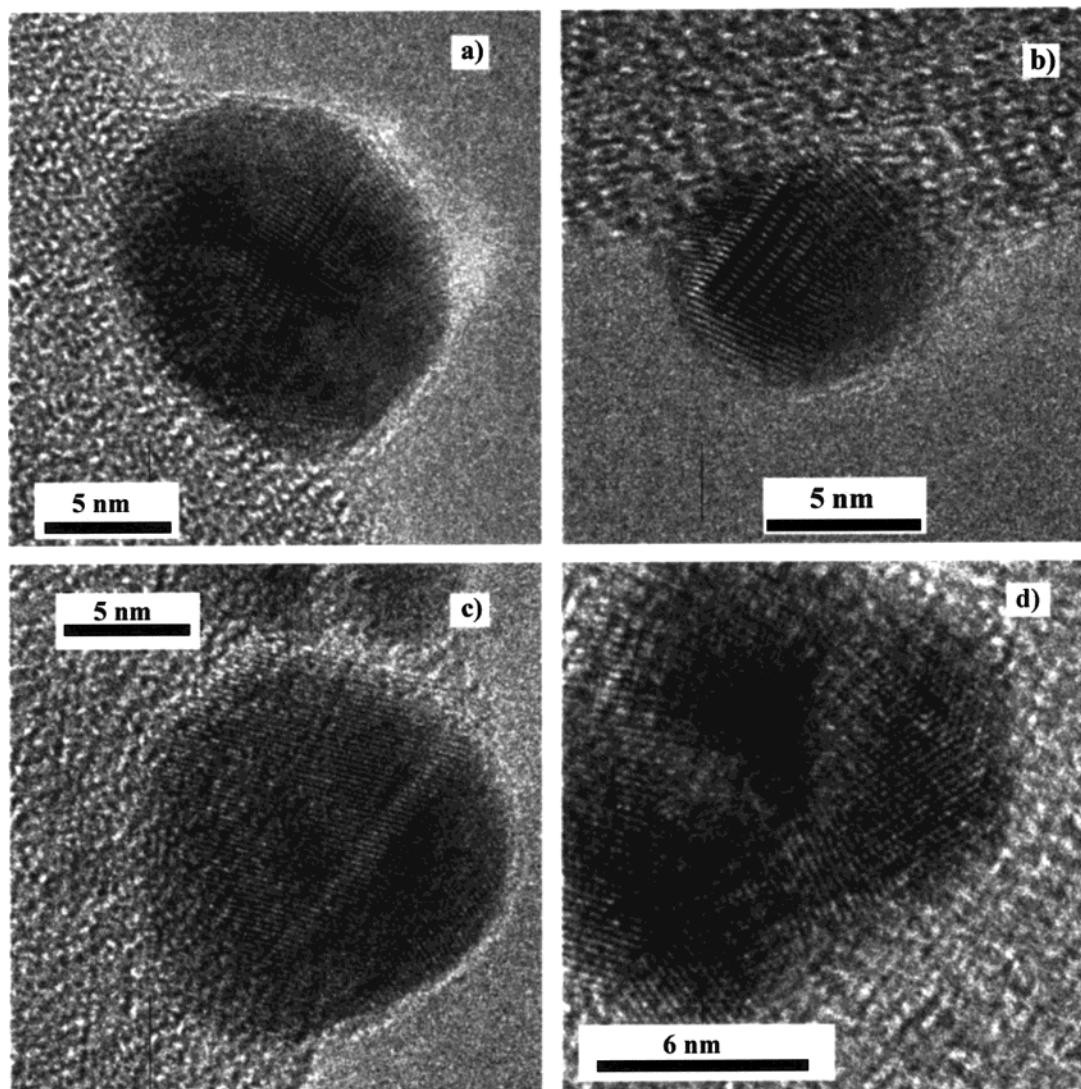


Figure 11. TEM images of polycrystalline silver nanocrystals coated with C₆F₁₃C₂H₄SH ligands synthesized in CO₂. (a)–(c) Multiple misaligned lattice fringes visible in nanocrystal core. (d) Coagulated nanocrystal with partial realignment of crystal planes.

carbon-coated nanocrystals represent the first synthesis of nanocrystals in pure CO₂. The nanocrystals can be redispersed in acetone and fluorinated solvents.

Because of the wide variety of available organometallic precursors soluble in *sc*-CO₂, and the large solubility of hydrogen, many different types of metal and semiconductor nanocrystals can feasibly be synthesized. The most effective precursors dissolve easily in CO₂, are stable at moderate temperatures, and must decompose quickly to the base metal with the addition of hydrogen. If hydrogen cannot reduce the precursor at moderate conditions, then higher temperatures or stronger reducing agents become necessary for particle formation. The nature of the binding group on the stabilizing ligand must also be considered when applying these methods to other materials. The stabilizing ligand must interact with the solvent to provide protection against irreversible aggregation and exhibit a binding strength weak enough to allow particle growth, yet strong enough to arrest particle growth in the nanometer size range.

Under the reaction conditions explored here, the precursor concentration predominantly determines the nanocrystal size with higher Ag(acac) concentrations, giving rise to larger particles. The average diameter ranged from as small as 26 Å to as large as 107 Å. The polydispersity, however, remained

constant, independent of nanocrystal size. Nondimensional analysis of the particle size distributions showed a self-similar solution, indicating consistency in the reaction mechanisms between the experiments. The log-normal shape of the size distributions, along with the polydispersity of the samples and the first and third moments of the size distributions indicate a growth mechanism that is dominated by coagulation between the nanocrystal cores. The perfluorooctanethiol capping ligand used in this study is unable to provide redispersibility in pure *sc*-CO₂ due to its length. The extremely low polarizability of *sc*-CO₂ results in approximately 50% larger van der Waals attractions for silver as compared with the case in conventional solvents. Partially because of this factor, C₈F₁₇C₂H₄SH ligands stabilize silver nanocrystals in pure CO₂ much more effectively than C₆F₁₃C₂H₄SH. In conclusion, the reaction method described here provides a pathway to the synthesis of metal nanocrystals with unique dispersibility characteristics in an environmentally benign solvent.

Acknowledgment. This work is supported in part by the STC Program of the National Science Foundation under Agreement No. CHE-9876674. We also acknowledge support from the Petroleum Research Fund, the Welch Foundation, and

the Separations Research Program at UT Austin. B.K. also thanks DuPont for partial support through a young professor grant. We also thank John Mendenhall at the Institute for Cell and Molecular Biology at UT Austin for TEM assistance.

References and Notes

- (1) Alivisatos, A. P. *Science* **1996**, *271*, 933–937.
- (2) Brust, M.; Walker, M.; Bethell, D.; Schiffrin, D. J.; Whyman, R. *J. Chem. Soc., Chem. Commun.* **1994**, 801–802.
- (3) Murray, C. B.; Norris, D. J.; Bawendi, M. G. *J. Am. Chem. Soc.* **1993**, *115*, 8706–8715.
- (4) Eckert, C. A.; Knutson, B. L.; Debenedetti, P. G. *Nature* **1996**, *383*, 313–318.
- (5) Johnston, K. P. *Curr. Opinion Colloid Interface Sci.* **2000**, *5*, 351–356.
- (6) Johnston, K. P.; DaRocha, S. R. P.; Holmes, J. D.; Jacobson, G. B.; Lee, C. T.; Yates, M. Z. *Interfacial Phenomena with CO₂-Soluble Surfactants*; DeSimone, J., Tumas, W., Eds.; Oxford University Press: Oxford, 2001.
- (7) Meredith, J. C.; Johnston, K. P. *Theory and Simulation of Colloid and Interface Science in Supercritical Fluids*; Kiran, E., Debenedetti, P., Peters, C., Eds.; Kluwer Academic Publishers: Dordrecht, The Netherlands, 2000; pp 211–228.
- (8) Meredith, J. C.; Johnston, K. P. *Macromolecules* **1998**, *31*, 5518–5528.
- (9) Peck, D. G.; Johnston, K. P. *Macromolecules* **1993**, *26*, 1537.
- (10) Meredith, J. C.; Sanchez, I. C.; Johnston, K. P.; de Pablo, J. J. *J. Chem. Phys.* **1998**, *109*, 6424–6434.
- (11) Yates, M. Z.; O'Neill, M. L.; Johnston, K. P.; Webber, S.; Canelas, D. A.; Betts, D. E.; DeSimone, J. M. *Macromolecules* **1997**, *30*, 5060–5067.
- (12) Lee, C. T.; Johnston, K. P.; Dai, H. J.; Cochran, H. D.; Melnichenko, Y. B.; Wignall, G. D. *J. Phys. Chem. B* **2001**, *105*, 3540–3548.
- (13) Hoefling, T. A.; Beitle, R. R.; Enick, R. M.; Beckman, E. J. *Fluid Phase Equilib.* **1993**, *83*, 203.
- (14) McClain, J. B.; Londono, D.; Combes, J. R.; Romack, T. J.; Canelas, D. A.; Betts, D. E.; Wignall, G. D.; Samulski, E. T.; DeSimone, J. M. *J. Am. Chem. Soc.* **1996**, *118*, 917–918.
- (15) O'Shea, K.; Kirmse, K.; Fox, M. A.; Johnston, K. P. *J. Phys. Chem.* **1991**, *95*, 7863.
- (16) O'Neill, M. L.; Yates, M. Z.; Johnston, K. P.; Smith, C. D.; Wilkinson, S. P. *Macromolecules* **1998**, *31*, 2838.
- (17) DeSimone, J. M.; Maury, E. E.; Menciloglu, Y. Z.; McClain, J. B.; Romack, T. J.; Combes, J. R. *Science* **1994**, *265*, 356.
- (18) Calvo, L.; Holmes, J. D.; Yates, M. Z.; Johnston, K. P. *J. Supercrit. Fluids* **2000**, *16*, 247–260.
- (19) Johnston, K. P.; Harrison, K. L.; Clarke, M. J.; Howdle, S. M.; Heitz, M. P.; Bright, F. V.; Carlier, C.; Randolph, T. W. *Science* **1996**, *271*, 624.
- (20) Ji, M.; Chen, X.; Wai, C. M.; Fulton, J. L. *J. Am. Chem. Soc.* **1999**, *121*, 2631–2632.
- (21) Holmes, J. D.; Bhargava, P. A.; Korgel, B. A.; Johnston, K. P. *Langmuir* **1999**, 6613–6615.
- (22) Silicon nanowires have been formed in supercritical hexane at 500 °C by utilizing gold seed crystals stabilized by thiol ligands. Holmes, J. D.; Johnston, K. P.; Doty, R. C.; Korgel, B. A. *Science* **2000**, *287*, 1471.
- (23) Shah, P. S.; Holmes, J. D.; Doty, R. C.; Johnston, K. P.; Korgel, B. A. *J. Am. Chem. Soc.* **2000**, *122*, 4245–4246.
- (24) Watkins, J. J.; McCarthy, T. J. *Chem. Mater.* **1995**, *7*, 1991–1994.
- (25) Watkins, J. J.; McCarthy, T. J. *Method of Chemically Depositing a Material onto a Substrate*; University of Massachusetts: Amherst, 1998.
- (26) Watkins, J. J.; Blackburn, J. M.; McCarthy, T. J. *Chem. Mater.* **1999**, *11*, 213–215.
- (27) Dryden, N. H.; Vittal, J. J.; Puddephatt, R. J. *Chem. Mater.* **1993**, *5*, 765–766.
- (28) Poliakov, M.; George, M. W.; Howdle, S. M. *Inorganic and Related Chemical Reactions in Supercritical Fluids*; Eldik, R. v., Hubbard, C. D., Eds.; Wiley: New York, 1997.
- (29) Darr, J. A.; Poliakov, M. *Chem. Rev.* **1999**, *99*, 495–541.
- (30) Korgel, B. A.; Fullam, S.; Connolly, S.; Fitzmaurice, D. *J. Phys. Chem. B* **1998**, *102*, 8379–8388.
- (31) Leff, D. V.; Ohara, P. C.; Heath, J. R.; Gelbart, W. M. *J. Phys. Chem.* **1995**, *99*, 7036–7041.
- (32) Previous studies using the biphasic approach have used thiol/precursor ratios less than 1.³⁰ Additionally, Brust found that well-capped gold nanocrystals, 10–30 Å in diameter, had a final thiol/gold ratio of 1:3.² Work by Leff showed that thermodynamic control over particle size could be obtained at thiol/precursor ratios between 1:1 and 6:1.³¹ This indicates that even at our lowest thiol/precursor ratio, there is an obvious molar excess of thiol.
- (33) Chidsey, C. E. D.; Loiacono, D. N. *Langmuir* **1990**, *6*, 682–691.
- (34) Bohren, C. F.; Huffman, D. R. *Absorption and Scattering of Light by Small Particles*; John Wiley & Sons: New York, 1983.
- (35) Hiemenz, P. C.; Rajagopalan, R. *Principles of Colloid and Surface Chemistry*, 3rd ed.; Marcel Dekker: New York, 1997.
- (36) Hamaker, H. C. *Physica* **1937**, *4*, 1058–1072.
- (37) Israelachvili, J. *Intermolecular & Surface Forces*, 2nd ed.; Academic Press: San Diego, 1992.
- (38) Korgel, B. A.; Fitzmaurice, D. *Phys. Rev. B* **1999**, *59*, 14191–14201.
- (39) *Fluorine Chemistry: A Comprehensive Treatment*; John Wiley & Sons: New York, 1995.
- (40) Chen, S.; Templeton, A. C.; Murray, R. W. *Langmuir* **2000**, *16*, 3543–3548.
- (41) Peng, X.; Wickham, J.; Alivisatos, A. P. *J. Am. Chem. Soc.* **1998**, *120*, 5343–5344.
- (42) Watzky, M. A.; Finke, R. G. *J. Am. Chem. Soc.* **1997**, *119*, 10382–10400.
- (43) Friedlander, S. K.; Wang, C. S. *J. Colloid Interface Sci.* **1966**, *22*, 126–132.
- (44) Pich, J.; Friedlander, S. K.; Lai, F. S. *Aerosol Sci.* **1970**, *1*, 115–126.
- (45) Swift, D. L.; Friedlander, S. K. *J. Colloid Science* **1964**, *19*, 621–647.
- (46) Reiss, H. *J. Chem. Phys.* **1951**, *19*, 482.
- (47) LaMer, V. K.; Dinegar, R. H. *J. Am. Chem. Soc.* **1950**, *72*, 4847.
- (48) Yacamán, M. J. Personal Communication.